THE ASTROPHYSICAL JOURNAL, 450:691–704, 1995 September 10

TEMPERATURE FLUCTUATIONS IN PHOTOIONIZED NEBULAE

J. B. KINGDON AND G. J. FERLAND
Department of Physics and Astronomy, University of Kentucky, Lexington, KY 40506
Received 1995 January 9; accepted 1995 March 22

ABSTRACT

Recombination lines in gaseous nebulae frequently yield parent-ion abundances that are several times larger than abundances derived from forbidden lines. One possible explanation for this discrepancy is the presence of temperature fluctuations. We examine temperature fluctuations in model nebulae by utilizing Peimbert's t^2 parameter. We have run large grids of models, varying the stellar temperature and the total hydrogen density. We consider two abundance sets: The first uses "typical" planetary nebulae abundances, while the second examines the effect of increasing the metals and grains by a factor of 3. We also consider both a constant density distribution and one which varies sinusoidally with radius. We examine the method of deriving t^2 observationally, which uses measured [O III] and Balmer temperatures. We find that this derived t^2 shows no correlation with the t^2 based on the integral definition. We discuss the reasons for this discrepancy, which include nonvalidity of some of the basic assumptions and theoretical and observational difficulties with the Balmer temperature. We find that, in high-metallicity objects especially, noncollisional contributions to [O III] λ4363 can significantly affect the derived temperature. We argue that while temperature fluctuations may result in non-negligible abundance corrections in some objects, they are insufficient to resolve the abundance discrepancy.

Subject headings: ISM: abundances — planetary nebulae: general

1. INTRODUCTION

Measurements of abundances in gaseous nebulae are essential for an understanding of stellar and galactic chemical evolution (Shields 1990; Aller 1990). When accurate atomic data are available, recombination-line intensities yield the best abundances because of their weak dependence on nebular temperature. However, many ions have weak or no recombination lines in observed spectra. In these cases, collisionally excited lines, with their exponential temperature dependence, must be used.

It has been known for many years now that for certain ions, abundances from forbidden lines often differ significantly from those derived from recombination lines (see Liu et al. 1995). The best known example is the long-standing discrepancy between the C III abundances predicted by C III] λ1909 and C II λ4267. A recent study of the planetary nebula (PN) NGC 7009 (Liu et al. 1995) has revealed significant discrepancies of this type for several ions. The authors derive recombination-line abundances of C, N, and O that are roughly 6, 4, and 5 times greater, respectively, than the corresponding forbidden-line abundances. The CNO recombination-line abundances are 2, 5, and 2 times solar, respectively. An extension of this study including six PNs (Barlow et al. 1995) yields values that are lower but still significant. The amplitude of these discrepancies is larger than the range in metallicity used to determine galactic abundance gradients or primordial He abundances. These results, therefore, cast doubt on the accuracy of any abundance determinations in gaseous nebulae, and these discrepancies must be understood before abundances can be given with certainty.

Several explanations have been proposed in order to resolve the above discrepancies. One idea is that the energy input to nebulae consists of some combination of photoionization and shocks (see Liu & Danziger 1993 for a discussion). While some evidence exists for shocks in some objects (see Middlemass et al. 1991), it is not known how prevalent this phenomenon is. An alternate explanation is nonuniform chemical abundances. Torres-Peimbert, Peimbert, & Peña (1990) were unable to obtain a good fit to both the C III] $\lambda\lambda$1907, 1909 lines and the C II λ4267 line in the PN NGC 4361 with a simple, homogeneous model. The fit was greatly improved with a two-zone model consisting of an inner, C-rich zone, and an outer, C-poor zone.

One of the oldest and most popular ideas involves the presence of temperature fluctuations (Peimbert 1967). Because of the different temperature dependence of forbidden and recombination lines, such fluctuations, if present and not accounted for in the derivation, will result in an underestimate of the forbidden-line abundances, while having little effect on the recombination-line abundances. The initial formalism for temperature fluctuations was developed by Peimbert (1967) in terms of the parameters T_0 and t^2, and was applied to abundance determinations by Rubin (1969).

There has been some debate over the magnitude of temperature fluctuations. Attempts to measure t^2 observationally (Rubin 1969; Torres-Peimbert, Peimbert, & Daltabuit 1980; Dinerstein, Lester, & Werner 1985) have resulted in a mean value of $t^2 = 0.035$. A more recent compilation by Liu & Danziger (1993) yields $t^2 = 0.03$, although the scatter is large. Conversely, Barker (1979) and Shaver et al. (1983) found no indication for appreciable temperature fluctuations in samples of PN and Galactic H II regions, respectively. Harrington et al. (1980) questioned the validity of large values of t^2 because of the difficulty in determining any physical process capable of producing such variations in a relatively small volume. A few attempts have been made to analyze this problem through the use of nebular models (Rubin 1969; Mihalszki & Ferland 1983; Harrington et al. 1982). These studies have focused on a very small number of objects or models. While the models demonstrate the existence of temperature fluctuations, they fail to reproduce values of t^2 as large as those derived from observations.

In order to better understand the behavior of temperature fluctuations, we compute here a large grid of photoionization models, covering a range of hydrogen density from log n_H = 2.25 to 6.00, and a range of stellar temperatures from log $T_{\rm eff}$ = 4.3 to 5.5. This range encompasses both H II regions and PNs. We consider both "typical" (generally metal deficient relative to the Sun) and metal-rich abundances and use two different density distributions. We also examine the effect of grains on our models. In addition to determining values of t^2 analytically for each model, we also compute a derived t^2 based on nebular temperatures from "observations" of the predicted emission spectrum.

In § 2, we give a brief review of the t^2 formalism including all pertinent equations. We also discuss some caveats in the use of derived nebular temperatures for determining t^2 observationally. We present our photoionization models and results in § 3. We discuss these results in detail in § 4 and summarize in § 5.

2. THEORETICAL AND OBSERVATIONAL CONSIDERATIONS

2.1. *Formalism*

We give here a brief overview of the formalism for temperature fluctuations. A much more rigorous discussion is presented by Peimbert (1967). In addition, many of the references above provide a brief treatment of the problem.

The intensity of a recombination line, or a collisionally excited line in the low-density limit where collisional de-excitation is negligible, can be written

$$I(\lambda) = \int n_e n_{\rm ion} \epsilon(T) dV \,, \tag{1}$$

where n_e and $n_{\rm ion}$ represent the electron and ion densities, respectively, and $\epsilon(T)$ is a function of temperature into which all appropriate constants have been absorbed. If temperature fluctuations are relatively small, we can expand the $\epsilon(T)$ term under the integral in a Taylor series about a mean temperature T_0, retaining only terms up to second order:

$$\epsilon(T) = \epsilon(T_0) + (T - T_0)\left(\frac{d\epsilon}{dT}\right)_{T_0} + \frac{1}{2}(T - T_0)^2\left(\frac{d^2\epsilon}{dT^2}\right)_{T_0} . \tag{2}$$

We may then judiciously choose the mean temperature T_0 such that

$$T_0 = \frac{\int T n_e n_{\rm ion} dV}{\int n_e n_{\rm ion} dV} \,, \tag{3}$$

which causes the first-order term in the expansion to vanish over the integral. If we further define

$$t^2 = \frac{\int (T - T_0)^2 n_e n_{\rm ion} dV}{T_0^2 \int n_e n_{\rm ion} dV} \,, \tag{4}$$

then equation (1) may then be rewritten as

$$I(\lambda) = \left[\epsilon(T_0) + \frac{1}{2}\left(\frac{d^2\epsilon}{dT^2}\right)_{T_0} T_0^2 t^2\right] \int n_e n_{\rm ion} dV \,. \tag{5}$$

The quantity $(t^2)^{1/2}$ is thus a rms deviation in temperature over a volume element, weighted by a density squared. We emphasize that each ion present in the nebula will have its own T_0 and t^2 as defined by the above equations.

From the above, it is clear that any temperature derived from nebular temperature indicators will be a function of the two parameters T_0 and t^2. Therefore, in order to observationally determine these parameters, it is necessary to use two temperature indicators with different temperature dependencies. The most common temperatures used in this analysis, because of their presence in the optical and relative ease of measurement, are the temperature derived from the [O III] λλ5007/4363 ratio [hereafter written as T(O III)], and that obtained from the ratio of the Balmer continuum to Hβ [hereafter T(Bal)]. A rigorous derivation using the above formalism yields

$$\mathrm{T(O\ III)} = T_0(\mathrm{O}^{+2})\left\{1 + \left[\frac{91280}{T_0(\mathrm{O}^{+2})} - 3\right]\frac{t^2(\mathrm{O}^{+2})}{2}\right\} \tag{6}$$

and

$$\mathrm{T(Bal)} = T_0(\mathrm{H}^+)[1 - 1.70 t^2(\mathrm{H}^+)] \,, \tag{7}$$

where we have explicitly denoted the dependence of T_0 and t^2 on the ion. We emphasize that equation (6) for T(O III) is only accurate when collisional de-excitation is negligible. If one measures both T(O III) and T(Bal), and makes the assumption that $T_0(\mathrm{O}^{+2}) \approx T_0(\mathrm{H}^+)$, and $t^2(\mathrm{O}^{+2}) \approx t^2(\mathrm{H}^+)$, then one uses equations (6) and (7) to solve for t^2. We shall return to the validity of this assumption later.

2.2. *Uncertainties in Temperature Measurement*

At this point, we wish to examine some of the difficulties incurred in deriving t^2 observationally as discussed in the previous subsection. We shall concentrate here on uncertainties in the measurement of T(Bal) and T(O III), and how these uncertainties affect the derived t^2.

2.2.1. *The Balmer Temperature*

There are several problems involved in accurately measuring the Balmer jump. Observationally, the main difficulty lies in determining the continuum redward of the discontinuity, which is hampered by the crowding of Balmer lines approaching the Balmer limit. A potentially greater source of uncertainty lies in comparison with theory. In order to compare the observed Balmer discontinuity with theoretical calculations, all other processes contributing to the observed continuum, such as He free-free and free-bound radiation, and H two-photon emission, must be calculated and subtracted. For some H II regions, scattered starlight from the ionizing star(s) further complicates the issue. Such processes will only be a problem if the continuum sources have an edge near the Balmer jump.

In Figure 1, we have plotted the quantity B/T(dT/dB) against T for a range of temperatures applicable to gaseous nebulae, based on the theoretical work of Ferland (1980). Here B is the ratio of the Balmer discontinuity to Hβ, and T is the derived Balmer temperature. From this plot, one can relate an uncertainty in the ratio B to the uncertainty in the derived temperature. Two points are worth noting. First, for a given error in B, the resulting error in T increases with increasing temperature. This is a direct result of the decreasing size of the Balmer jump with temperature, which causes greater uncertainties in measurement. Second, the values on the y-axis, which multiply an uncertainty in B to produce the resulting uncertainty in the derived temperature, are all greater than 1. Thus, any uncertainty in the measured Balmer discontinuity to

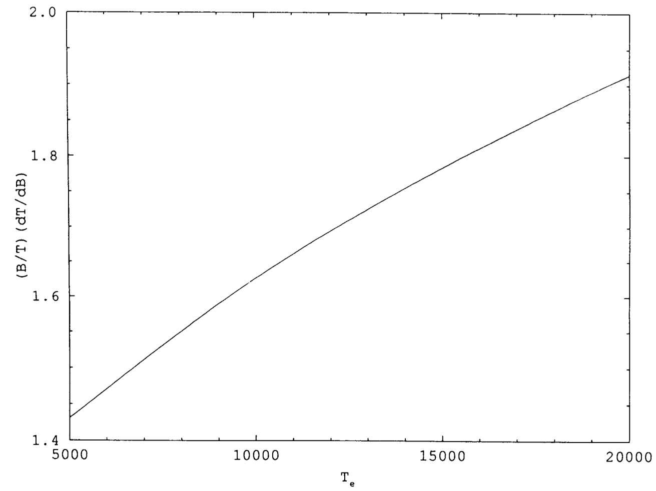

FIG. 1.—Factor relating a given error in B (the ratio of the Balmer discontinuity to Hβ) to the resulting error in the temperature T as a function of T.

Hβ ratio will result in a *larger* uncertainty in the Balmer temperature.

To quantify these ideas, we refer to the work of Liu & Danziger (1993). These authors present Balmer temperatures and their corresponding uncertainties for 14 PNs. From their list, we find an average Balmer temperature uncertainty of $\sim 18\%$. In conclusion, we find that the Balmer temperature can have substantial uncertainties, which will affect the derived value of t^2.

2.2.2. *The* [O III] *Temperature*

In general, uncertainties in T(O III) are smaller than those for T(Bal). Observationally, the greatest problem lies in the large difference in intensity between $I(5007)$ and $I(4363)$. For low-excitation objects in particular, $I(4363)$ can be quite weak.

Another potential source of uncertainty is noncollisional enhancement of $\lambda 4363$ (see Rubin 1986 for a general discussion of noncollisional effects in forbidden lines). We shall briefly consider two sources of enhancement here: charge transfer and recombination.

The charge transfer reaction $O^{+3} + H \rightarrow O^{+2} + H^+$ predominantly populates the $2p3p\ ^1P$ and $2p3s\ ^1P^o$ states of O^{+2} (Dalgarno & Sternberg 1982). These levels then cascade downward to the ^1S and ^1D levels from which $\lambda 4363$ and $\lambda 5007$ arise. Generally, this process is negligible in nebulae compared to collisional excitation, but it may reach a few percent of the total in some cases.

The ratio of the $\lambda 4363$ intensity due to recombination to that due to collisional excitation is given in the low-density limit by

$$\frac{I_{\rm rec}(4363)}{I_{\rm coll}(4363)} = \left(\frac{n_{O^{+3}}}{n_{O^{+2}}}\right) \frac{\alpha^{\rm eff}(4363)}{q} , \quad (8)$$

where all symbols have their usual meaning. The relative importance of recombination thus depends on the relative ionization through the first term on the right-hand side in the above equation, and on the temperature through the second term. Because of the exponential temperature dependence of collisional excitation, recombination, as well as charge transfer, becomes increasingly important at low temperatures. For cases in which noncollisional processes are important, T(O III) derived in the usual way will be overestimated. This, in turn, will lead to an underestimate of the abundance. We show below that such processes can amount to as much as 20% of the total 4363 intensity.

2.2.3. *Uncertainties in the Derived* t^2

We now consider how the uncertainties in T(Bal) and T(O III) discussed above will affect the derived t^2. In order to rigorously derive the uncertainty in t^2, it would be necessary to solve equations (6) and (7), propagating the errors throughout. We shall take a simpler approach, which will provide a qualitative feel for the magnitude of the uncertainty.

Let us assume that we have solved equations (6) and (7) for T_0 and have obtained an accompanying uncertainty σ_{T_0} by propagating the uncertainties in both T(Bal) and T(O III) through the equations. We then substitute these values into equation (7) to solve for t^2. Letting σ_{t^2} be the uncertainty in the value of t^2 derived this way, standard error analysis yields

$$\sigma_{t^2} \approx \frac{1}{2} \frac{\sigma_{T_0}}{T_0} . \quad (9)$$

As a case in point, let us assume that the derived T_0 has a relative uncertainty of 15%, based on the discussion in the two previous sections. Then $\sigma_{t^2} = 0.075$. This value is 2.5 times the canonical value $t^2 = 0.30$ mentioned in § 1. While the above derivation is not rigorous, it suggests that relatively small uncertainties in T(Bal) and T(O III) can result in significant uncertainties in the derived t^2. That this is in fact true can be seen by examining Figure 2 of Liu & Danziger (1993), where temperature error bars intersect values of t^2 covering about half an order of magnitude. This casts some doubt on the validity of values of t^2 derived in this way. We shall return to this point later.

Finally, we note that roughly 40% of the objects in Liu & Danziger (1993) have a derived value of t^2 which is negative. Obviously, a negative t^2 has no physical meaning. If such values are purely because of propagated errors as discussed above, we would expect negative values of t^2 roughly half the time.

3. MODELS

In the previous section, we presented the methodology to derive t^2. In this section, we compute a large number of photoionization models in order to understand the behavior of t^2 with nebular and stellar parameters, and to determine an estimate of its magnitude. We use the photoionization code Cloudy (Ferland 1994). This code treats both ionization and thermal balance self-consistently. For each model, we determine t^2 in two ways. First, we utilize the direct definition (eq. [4]), using H^+ as the zone to be integrated over. Second, we use model-predicted intensities of [O III] $\lambda\lambda 4363$, 5007 and the Balmer discontinuity and Hβ to derive T(O III) and T(Bal). We then calculate t^2 using equations (6) and (7). For clarity, we shall hereafter refer to the value of t^2 derived from equation (4) as $t^2_{\rm str}$ and that derived from T(O III) and T(Bal) as $t^2_{\rm obs}$. Since equation (7) is only strictly valid when collisional de-excitation of the [O III] lines is unimportant, we restrict our determination of $t^2_{\rm obs}$ to $\log n_e \leq 4.25$. For temperatures typical in gaseous nebulae, this will ensure that collisonal de-excitation is negligible. We present the models and their results below.

3.1. *Constant Density Models*

For these models, the total hydrogen density $n_{\rm H}$ (defined as $n_{\rm H} = n_p + n_{\rm H^0}$) is taken to be constant across the nebula. We compute large grids of models by varying the total hydrogen density and the stellar temperature $T_{\rm eff}$ within the ranges $\log n_{\rm H} = 2.25$–6.00, and $\log T_{\rm eff} = 4.3$–5.5. This range encompasses both H II regions and PNs.

For all models, we consider the geometry to be spherically symmetric, with a distance between the ionizing source and the ionized cloud face equal to 10^{17} cm. For the range of densities considered here, this results in models ranging from spherical through plane parallel. The ionizing source is taken to be a blackbody with a total luminosity of 10^{38} ergs $\rm s^{-1}$. All models are stopped at the H ionization front; thus, they are ionization bounded. We note here that stopping the models before the ionization front (i.e., having density-bounded models) would result in smaller values of $t^2_{\rm str}$. We use two different abundance sets. These abundances, and the results of the grids, are described below.

3.1.1. *PN Abundances*

For our initial abundance set, we consider "typical" PN abundances. These are essentially a mean of abundances determined from a large number of PNs by Aller & Czyzak (1983), with small values for elements not listed by them. The abundances, relative to H, are given in Table 1 and are generally below solar values. While these abundances are taken from PNs, the results of our models should be equally applicable to H II regions. We also include grains and their effects on the thermal and ionization equilibrium of the nebula (see Baldwin et al. 1991) from unpublished data by K. Volk, which are based on observations of post–asymptotic giant branch stars. We take the dust-to-gas ratio to be equal to that of the general interstellar medium (see Mallik & Peimbert 1988). Using these abundances and grains, plus the parameters discussed in the previous section, we have computed a grid of roughly 800 model nebulae.

In Figure 2, we present a contour plot of $t^2_{\rm str}$ as a function of $n_{\rm H}$ and $T_{\rm eff}$ for the PN grid. We shall focus on two points of interest here. First, we note that in general, for low to moderate densities, there is little dependence of $t^2_{\rm str}$ on $n_{\rm H}$, and a strong

TABLE 1

PLANETARY NEBULA GRID ABUNDANCES

Atom	Abundance
He	0.10
C........	7.8(−4)
N	1.8(−4)
O	4.4(−4)
Ne	1.1(−4)
Na	3.0(−7)
Mg......	1.6(−6)
Al	2.2(−7)
Si	1.0(−5)
S	1.0(−5)
Cl	1.7(−7)
Ar.......	2.7(−6)
Ca	1.2(−8)
Fe.......	5.0(−7)
Co	1.0(−9)
Ni.......	1.8(−8)

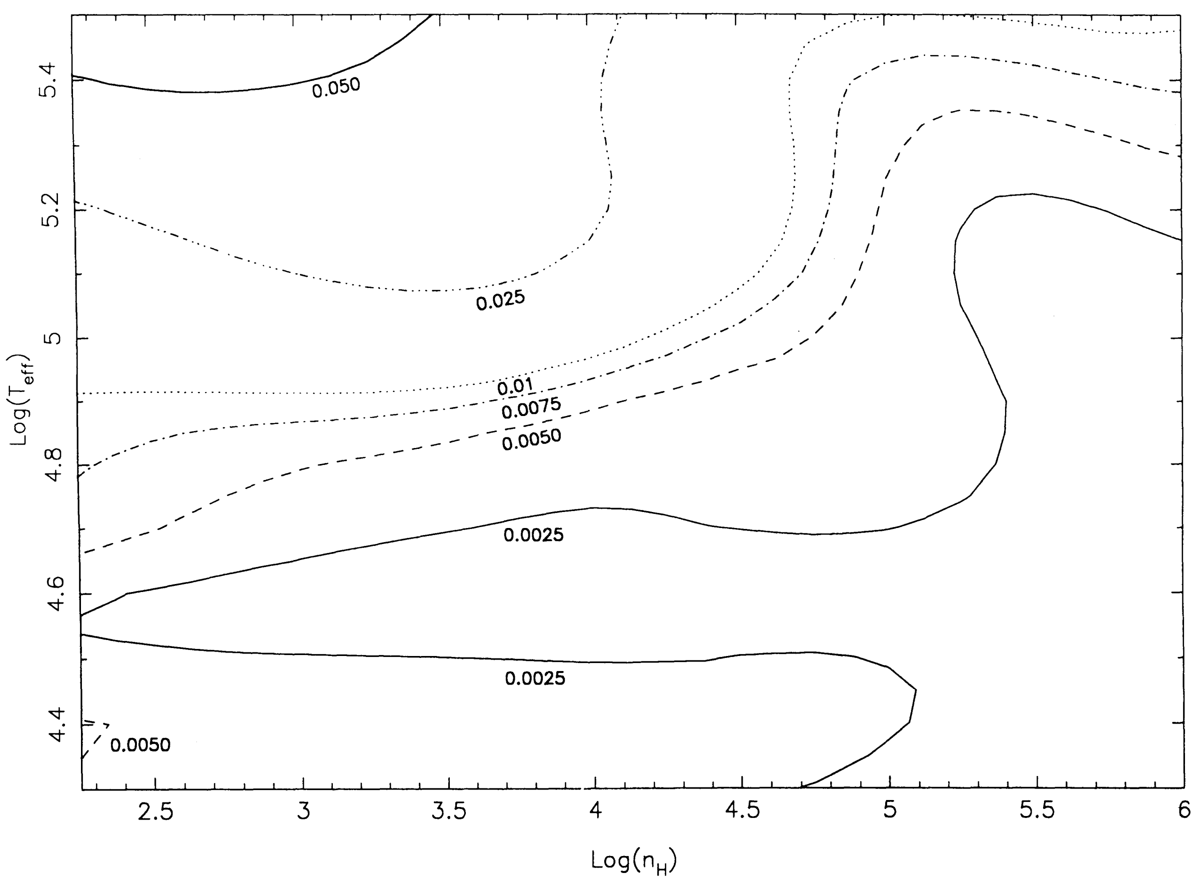

FIG. 2.—Contour plot of $t^2_{\rm str}$ for the PN grid

dependence at high densities. This effect is due to sphericity. Because the H^+ Strömgren depth decreases with increasing density, the models progress from a spherical geometry to a thick shell, to models that are essentially plane parallel as density increases. At high densities, the change in the thickness of the ionized zone with increasing density becomes a significant fraction of the Strömgren depth. This causes $t^2_{\rm str}$ to decrease through the volume element in equation (4).

Second, there is a general trend for $t^2_{\rm str}$ to increase with decreasing density and increasing stellar temperature. The mean ionization of the nebula shows the same trend. For high $T_{\rm eff}$, the incident photon flux is very hard. This, coupled with the low density, results in very high ionization at the ionized face, producing significant heating through photoionization. Thus, nebulae in this regime have very high nebular temperatures at the ionized face. These temperatures then fall off relatively quickly with radius, resulting in large temperature variations over the nebula. The slight deviation from this trend at low $T_{\rm eff}$ is related to the size and location of the O^{+2} zone. This zone affects the nebular temperature through collisional cooling.

In order to assess the importance of grains on these results, we have run another grid, identical to that described above, except that grains are not included. We have left the gas-phase abundances of all elements unchanged. The analogous plot to Figure 2 is shown in Figure 3. From a comparison of these two figures, it can be seen that the absence of grains decreases $t^2_{\rm str}$ by roughly a factor of 2. This is due to the fact that grains provide a net heating source, particularly in the inner regions of the nebula (see Kingdon & Ferland 1993; Baldwin et al. 1991; Borkowski & Harrington 1991; Harrington, Monk, & Clegg 1988). However, the grains do *not* affect the general behavior of $t^2_{\rm str}$ with $n_{\rm H}$ and $T_{\rm eff}$.

Figure 4 depicts a contour plot of $t^2_{\rm obs}$ for the PN grid, using the high-density cutoff discussed above. As was the case for $t^2_{\rm str}$, it can be seen that $t^2_{\rm obs}$ shows little dependence on density. We draw attention to the contours in Figure 4 with negative values. Negative values of $t^2_{\rm obs}$ will occur whenever T(O III) < T(Bal), as can be seen from equations (6) and (7).

A comparison between Figures 2 and 4 will show that the contours of $t^2_{\rm str}$ and $t^2_{\rm obs}$ do not generally coincide. To make this clearer, we plot in Figure 5 the difference $t^2_{\rm obs} - t^2_{\rm str}$. The range of good agreement occurs for low stellar temperatures typical of H II regions, with the discrepancy increasing with increasing $T_{\rm eff}$. It is essential that we understand this discrepancy, as Figure 5 clearly shows that, for a wide range of nebulae, using $t^2_{\rm obs}$ to correct abundances for temperature fluctuations will produce erroneous results.

We first consider the uncertainties in $t^2_{\rm obs}$ discussed in § 2.2. We can immediately exclude observational errors in T(O III) and T(Bal), as these are calculated using model-predicted line and continuum intensities. On the theoretical side, we have made every attempt to accurately account for all processes contributing to the continuum over the Balmer discontinuity. In order to assess the importance of noncollisional effects in the [O III] lines, we have computed the noncollisional contribution to λ4363 for each model in our grid. The results are shown in Figure 6. Although the behavior of noncollisonal

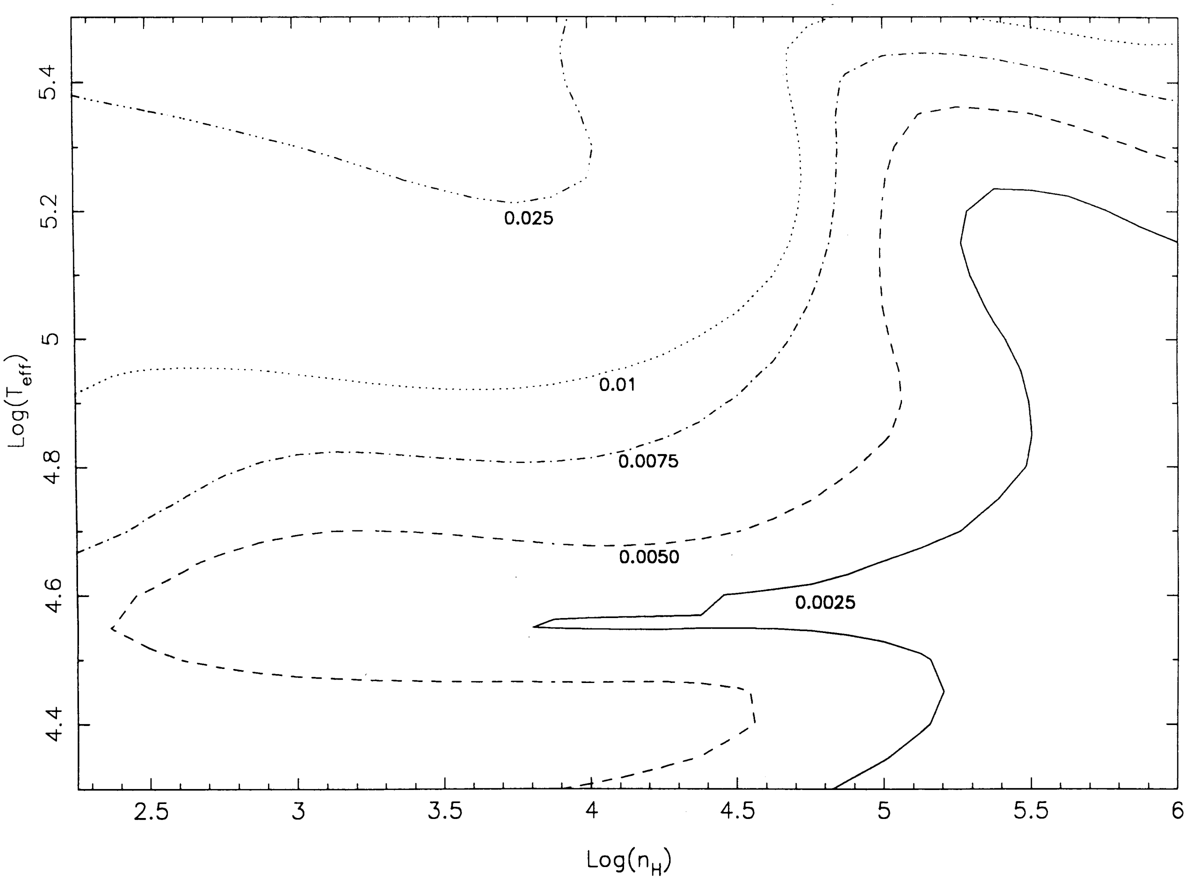

FIG. 3.—Same as Fig. 2, but for a model without grains

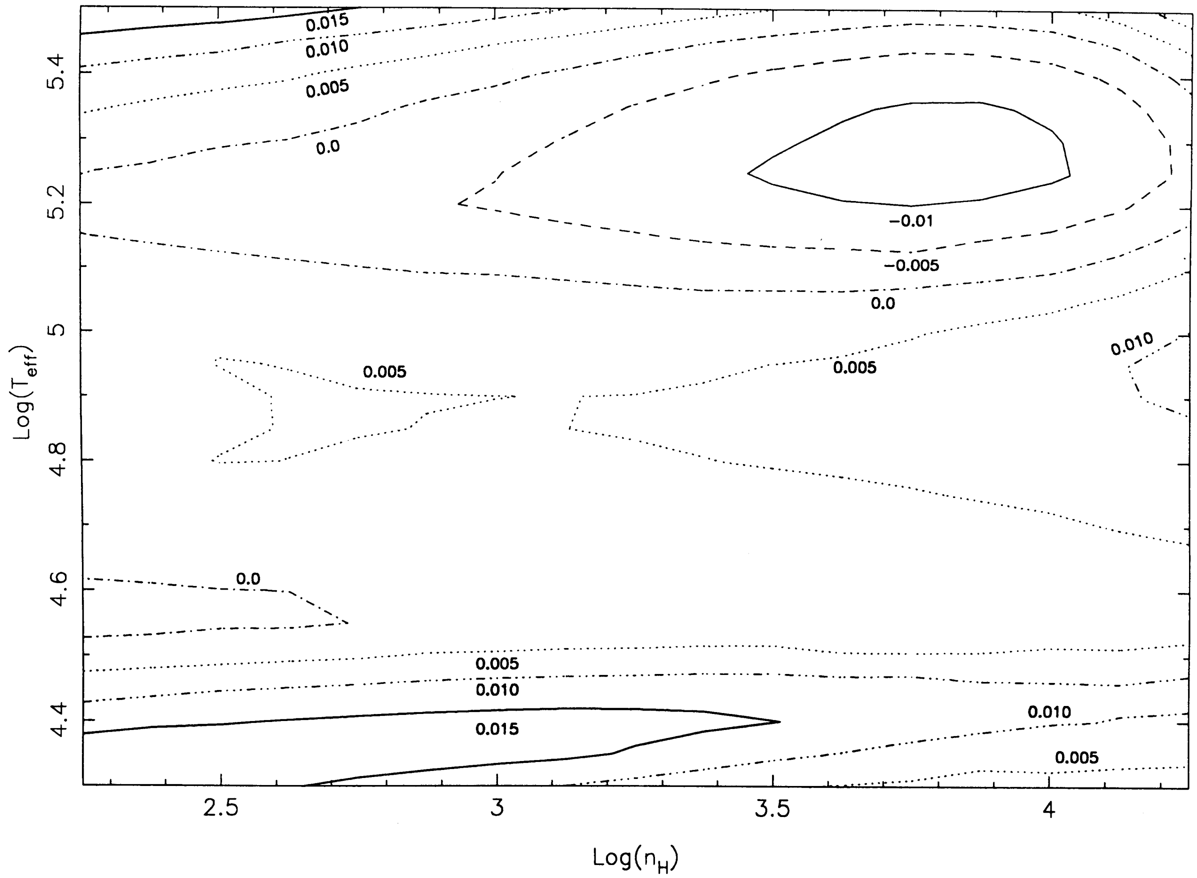

FIG. 4.—Contour plot of $t^2_{\rm obs}$ for the PN grid

effects with $T_{\rm eff}$ is similar to the trend in Figure 5, the magnitude of the effect is insufficient to explain the $t^2_{\rm obs}$–$t^2_{\rm str}$ discrepancy. We further note that no random systematic error can explain the discrepancy, as such errors should cause as many values of $t^2_{\rm obs} < t^2_{\rm str}$ as $t^2_{\rm obs} > t^2_{\rm str}$, whereas Figure 5 clearly shows a bias toward $t^2_{\rm obs} < t^2_{\rm str}$.

Since we are unable to resolve this discrepancy by appealing to errors in the parameters, we must examine the methodology itself. The major assumption underlying the derivation of $t^2_{\rm obs}$ is that $T_0(O^{+2}) \approx T_0(H^+)$, and $t^2(O^{+2}) \approx t^2(H^+)$. We might expect that these approximations will be valid for nebulae in which the O^{+2} zone nearly fills the H^+ Strömgren sphere, and to be somewhat doubtful otherwise. Indeed, the condition that O is almost completely O^{+2} was the situation for Model 1 of Rubin (1969), for which $t^2(O^{+2}) \approx t^2(H^+)$ was satisfied. To quantify these ideas, we present in Figure 7 a plot of the difference $T_0(O^{+2}) - T_0(H^+)$ for the PN grid, where both mean temperatures have been computed using the definition of equation (3). This difference must be zero for the methodology to be valid. From this figure, we see that the approximation is reasonably valid for low $T_{\rm eff}$, and becomes increasingly worse for higher stellar temperatures. Indeed, at high $T_{\rm eff}$, the difference may amount to as much as 10% of the magnitude of T_0. This behavior matches that of Figure 5. A comparison of the two plots shows that when $T_0(O^{+2}) \approx T_0(H^+)$, so that our assumption is valid, then $t^2_{\rm obs} \approx t^2_{\rm str}$. These results suggest that the methodology for deriving t^2 from observations is only reasonable within a fairly limited range of stellar temperatures. Most importantly, any values of $t^2_{\rm obs}$ presented for objects with very hot central stars (such as PNs) should be viewed with extreme skepticism.

3.1.2. *High-Metallicity Grid*

For our second abundance set, we wish to examine the effect of metallicity on t^2. This is prompted by the high metallicities found in NGC 7009 by Liu et al. (1995). We create a high-metallicity grid by multiplying all metal and grain abundances from the PN grid by a factor of 3. All other parameters remain the same.

Figure 8 shows a contour plot of $t^2_{\rm str}$ for the high-metallicity grid. The general trend of increasing $t^2_{\rm str}$ with increasing $T_{\rm eff}$ and decreasing $n_{\rm H}$ is the same as for the PN grid. The main difference is that for most points, the value of $t^2_{\rm str}$ is larger in the high-metallicity grid than in the PN grid. This difference increases with increasing $t^2_{\rm str}$, reaching a maximum of a factor of ~2.

In order to understand this behavior, we must consider the thermal balance at an arbitrary point in the nebula. It is well known that increasing metallicity will result in increased cooling via enhanced collisional line radiation. This process lowers the nebular temperature (see, e.g., Stasińska 1980 for a discussion of temperature effects in high-metallicity H II regions). However, the increased metallicity also results in increased grain opacity, which causes increased heating through photoionization. This in turn raises the nebular temperature. The net effect of these two processes is that the temperature at any point in the high-metallicity nebula is only slightly lower than that for the "normal" metallicity nebula.

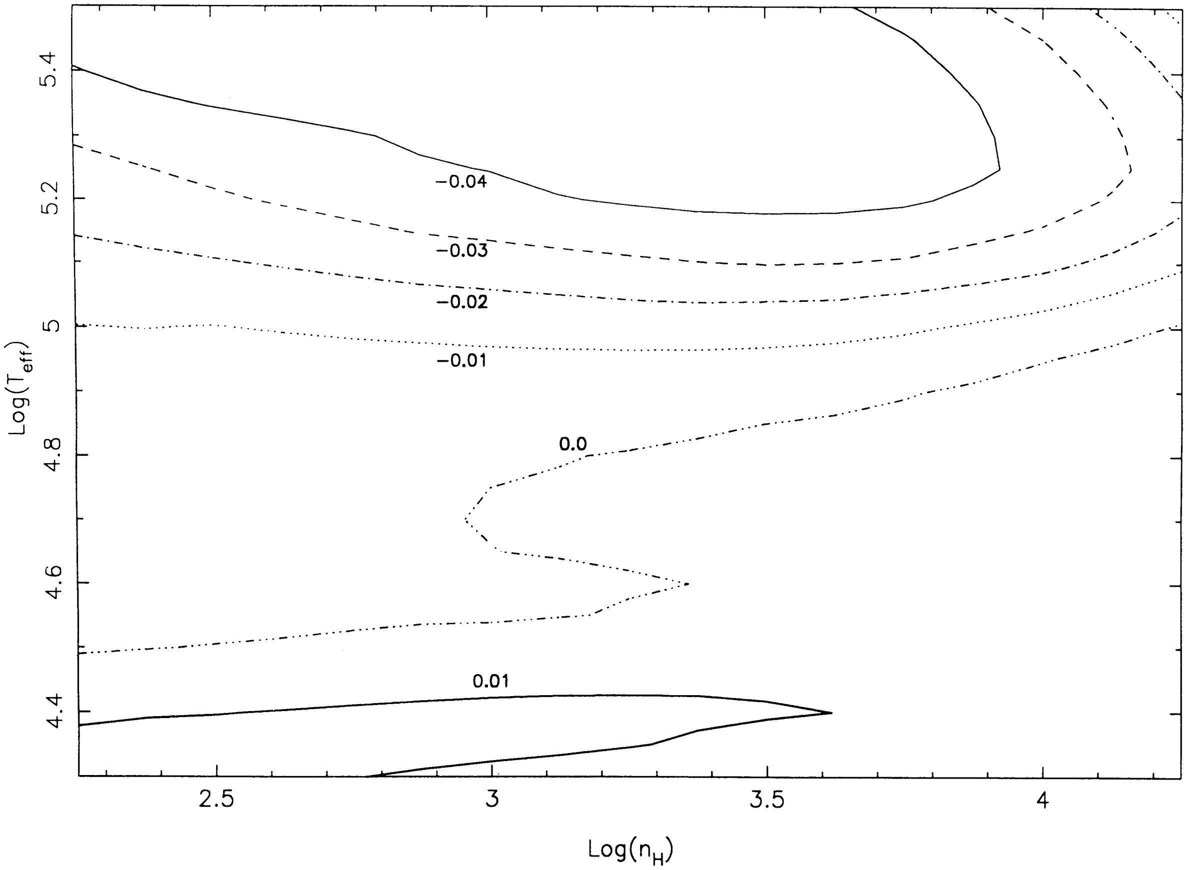

FIG. 5.—Contour plot of the difference $t^2_{\rm obs} - t^2_{\rm str}$ for the PN grid

However, the increased opacity causes the photon flux to fall off more quickly with radius. This produces a sharper gradient in dT/dR, resulting in a larger value of $t^2_{\rm str}$. This effect is more pronounced at low densities and high stellar temperatures, because metals make a greater contribution to the opacity in this regime. For low $T_{\rm eff}$, the incident photon flux is relatively soft, H and He can absorb the bulk of the radiation, and the addition of metals has little effect. Similarly, because opacity is proportional to density, metal opacity is not as important at high $n_{\rm H}$.

In Figure 9 we plot the quantity $t^2_{\rm obs} - t^2_{\rm str}$ for this grid. The behavior is essentially identical to Figure 5, the analogous plot of the PN grid, except that the magnitude of the discrepancy is larger. Since metallicity has essentially no effect on the basic assumptions needed to derive $t^2_{\rm obs}$, this discrepancy can be described in exactly the same way as that for the PN grid. We plot the difference $T_0(\rm O^{+2}) - T_0(\rm H^+)$ in Figure 10. Again, this plot is nearly identical in form to Figure 7 except that the value of the difference is generally greater. The larger differences correspond to the larger discrepancies in $t^2_{\rm obs} - t^2_{\rm str}$ in Figure 9.

Although the $t^2_{\rm obs} - t^2_{\rm str}$ discrepancy can be largely explained by nonvalidity of the basic assumptions for obtaining $t^2_{\rm obs}$, noncollisional effects in [O III] also make a contribution. In Figure 11 we plot the percentage of [O III] λ4363 due to noncollisional processes. The values here are larger than those in Figure 6, the analogous plot for the PN grid, because of the generally lower nebular temperatures in this grid. It is evident from this figure that nebular temperatures derived from the [O III] lines for high-metallicity objects can be significantly overestimated if noncollisional processes are not considered. This will result in abundances being underestimated.

3.2. *Variable Density Models*

In the previous sections, we found that for constant density models, large values of t^2 only occur for nebulae with high $T_{\rm eff}$ and low $n_{\rm H}$. In this section, we investigate how a variable density will affect our results. Variations in density can create variations in nebular temperature, although the magnitude of the temperature variations is much less than those in the density (see Rubin 1989).

For illustrative purposes, we shall consider models in which the ionizing source is a blackbody with log $T_{\rm eff} = 4.85$. We use the high-metallicity abundances of the previous section, as these resulted in the largest values of t^2. Our geometry is again spherical with an inner radius of 10^{17} cm. For our density distribution, we consider the sinsusoidal model of Mihalszki & Ferland (1983). The total hydrogen density $n_{\rm H}$ is expressed as

$$n_{\rm H} = \left(\frac{n_{\rm max} - n_{\rm min}}{2}\right) \cos \delta r + \left(\frac{n_{\rm max} + n_{\rm min}}{2}\right), \quad (10)$$

where $n_{\rm max}$ and $n_{\rm min}$ are the maximum and minimum densities considered, respectively, r is the depth into the nebula in cm, and δ is equal to 2π divided by the period (in cm) of the oscillations. Although a sinsusoidal density distribution has no physical basis, it will serve to illustrate the effect of density fluctuations on t^2.

For our models, we consider all combinations of $n_{\rm max}$ and $n_{\rm min}$ between 10^2 cm^{-3} and 10^6 cm^{-3}, with the proviso that all

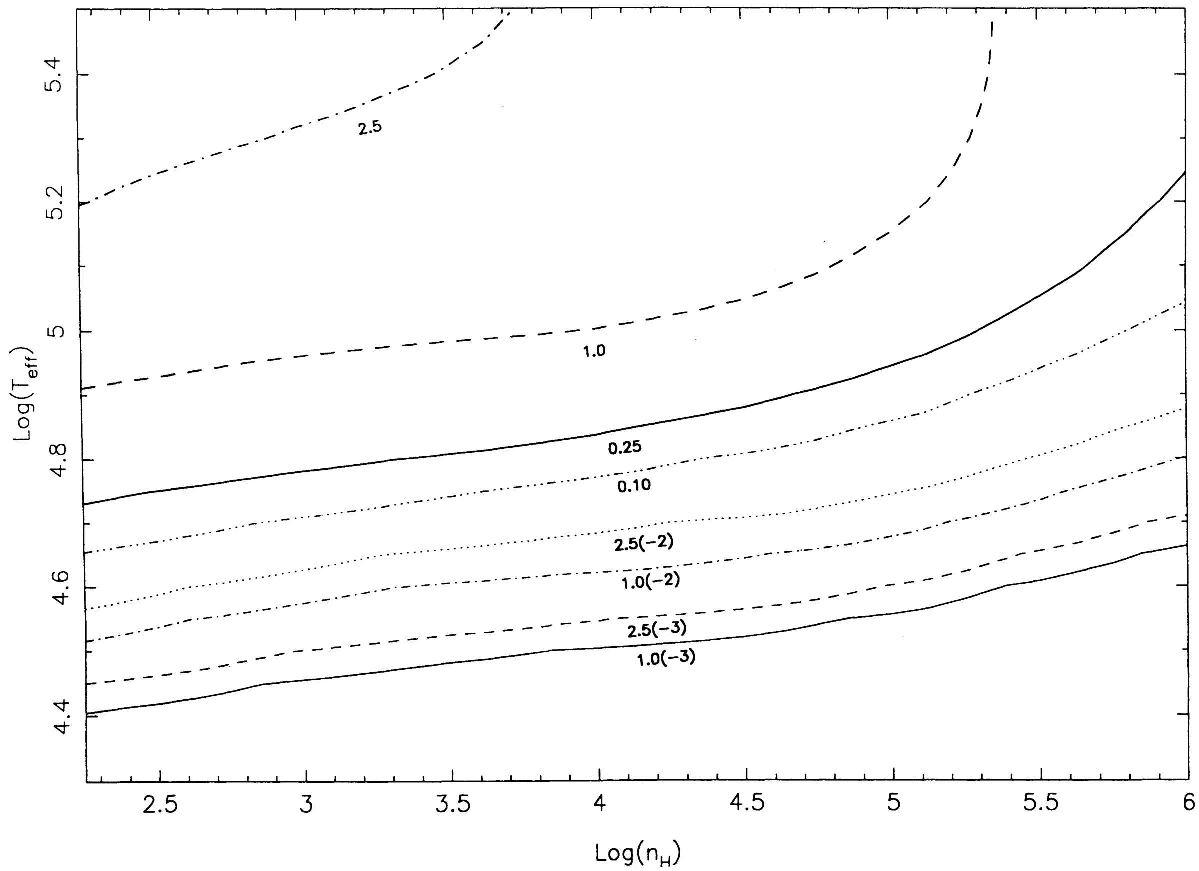

FIG. 6.—Percentage of the [O III] λ4363 intensity due to noncollisional processes for the PN grid

densities be expressable as integer powers of 10. For each ($n_{\rm max}$, $n_{\rm min}$) pair, we also compute results for several values of the period.

We present the results of our calculations in Table 2. The first and second columns list the minimum and maximum density for the model, respectively. The third column gives the number of periods of the function per Strömgren radius. We have listed the minimum and maximum period considered for each ($n_{\rm max}$, $n_{\rm min}$) pair. We give the derived $t^2_{\rm str}$ in the fourth column. We have not listed $t^2_{\rm obs}$, as the results of the previous sections show that this value is generally meaningless. An example of the effect of the density variations on the temperature is depicted in Figure 12, which shows the nebular temperature as a function of the log of the nebular radius for the second model listed in Table 2.

It is evident from Table 2 that sinsusoidal models do not, in general, result in large values of $t^2_{\rm str}$. As in the constant density models, there is a trend of decreasing $t^2_{\rm str}$ with increasing mean density. We note that models with the same value for $n_{\rm max}$ but different $n_{\rm min}$ have similar values of $t^2_{\rm str}$. This suggests that $t^2_{\rm str}$ is determined mainly by the maximum density obtained in the model. To verify this, for each $n_{\rm max}$ we have computed a constant density model with $n_{\rm H} = n_{\rm max}$, using the high-metallicity abundances and log $T_{\rm eff} = 4.85$. Our results, denoted by $t^2_{\rm max}$, appear in the fifth column of Table 2. For low densities, a comparison between $t^2_{\rm str}$ and $t^2_{\rm max}$ is hampered by sphericity effects, which result in significantly smaller Strömgren radii for the sinusoidal models as compared with the analogous constant density models. Taking this effect into account, we find that $t^2_{\rm str}$ is always somewhat larger than $t^2_{\rm max}$, with the greatest differences occurring at the highest densities, where $t^2_{\rm str}$ is smallest.

The dependence of $t^2_{\rm str}$ on $n_{\rm max}$, and its near independence on $n_{\rm min}$ is due to the fact that $t^2_{\rm str}$ is weighted by an effective density squared term. Therefore, in nebulae with a nonconstant density distribution, the high-density regions will contribute preferentially to the derived $t^2_{\rm str}$. In effect, although density fluctuations can cause fluctuations in temperature, $t^2_{\rm str}$ will not

TABLE 2

RESULTS OF SINUSOIDAL MODELS

$n_{\rm min}$	$n_{\rm max}$	R_s/P	$t^2_{\rm str}$	$t^2_{\rm max}$
10^2......	10^3	0.69	2.64(−2)	1.96(−2)
10^2......	10^3	16.67	1.89(−2)	1.96(−2)
10^2......	10^4	0.81	7.49(−3)	6.72(−3)
10^2......	10^4	4.55	9.28(−3)	6.72(−3)
10^2......	10^5	0.85	2.86(−3)	3.19(−3)
10^2......	10^5	3.13	3.44(−3)	3.19(−3)
10^2......	10^6	0.86	7.14(−4)	7.03(−4)
10^2......	10^6	2.94	1.63(−3)	7.03(−4)
10^3......	10^4	0.78	7.15(−3)	6.72(−3)
10^3......	10^4	11.11	9.30(−3)	6.72(−3)
10^3......	10^5	0.85	2.83(−3)	3.19(−3)
10^3......	10^5	6.67	3.46(−3)	3.19(−3)
10^3......	10^6	0.86	7.12(−4)	7.03(−4)
10^3......	10^6	2.94	1.64(−3)	7.03(−4)
10^4......	10^5	0.81	2.55(−3)	3.19(−3)
10^4......	10^5	12.50	3.34(−3)	3.19(−3)
10^4......	10^6	0.86	6.97(−4)	7.03(−4)
10^4......	10^6	7.14	1.51(−3)	7.03(−4)
10^5......	10^6	0.82	5.26(−3)	7.03(−4)
10^5......	10^6	12.50	1.56(−3)	7.03(−4)

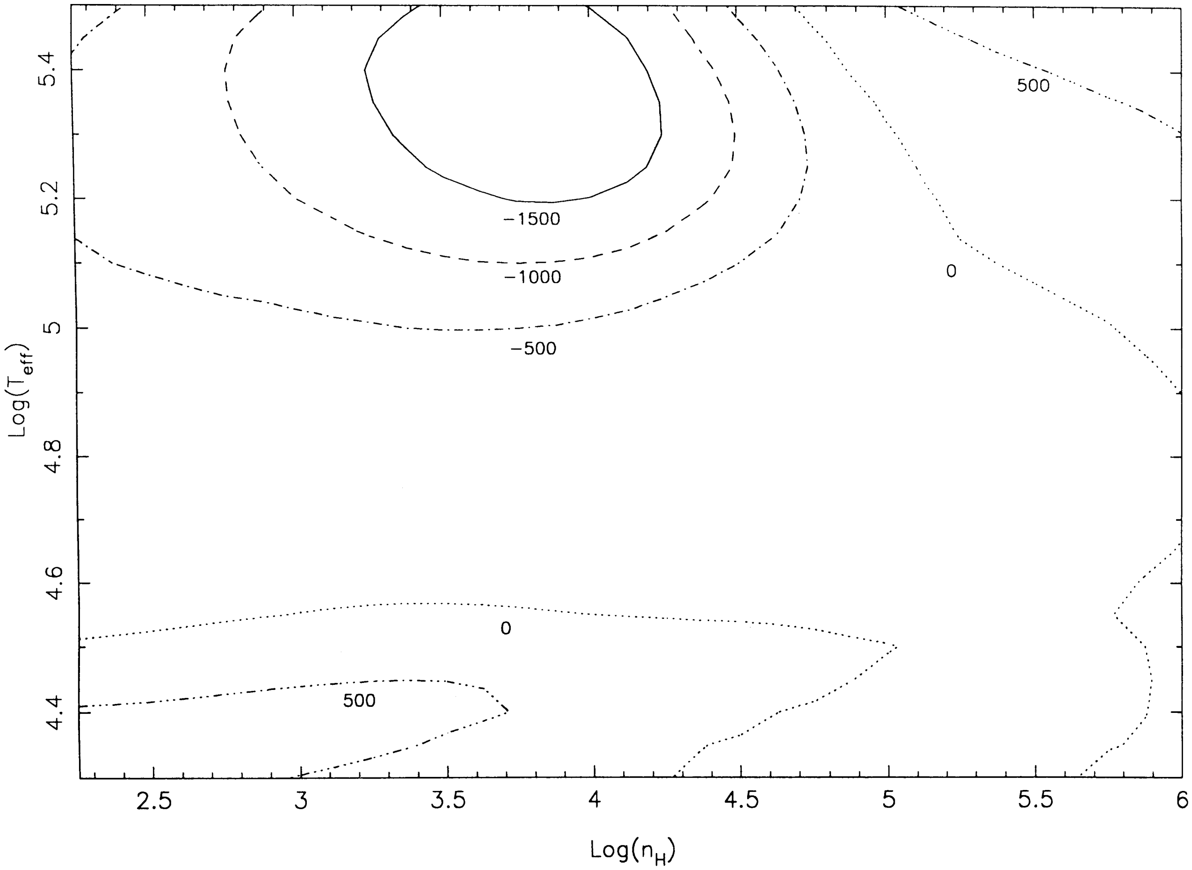

FIG. 7.—Contour plot of the difference $T_0(O^{+2}) - T_0(H^+)$ for the PN grid

"see" temperatures occurring in the low-density regions, and will essentially trace only the temperature in the high-density zones.

One way to avoid this problem is to imagine a density distribution in which the high-density regions occupy a smaller volume than the low-density regions. We consider a density distribution given by

$$n_H = n_0\left(\frac{d_0}{d_0 - d}\right)^{\alpha}, \qquad (11)$$

where n_0 is the minimum density, occurring at the ionized face, d is the depth into the nebula (distance from the central star minus the inner radius), and d_0 is a scaling distance at which the density becomes infinite. This is essentially the density law of Williams (1992), used to describe dense condensations in nebulae. According to Williams, if $\alpha = 1.5$, all density regimes will be weighted equally, thus removing the high-density bias encountered in the sinusoidal models. We have run a series of models to examine the effect of this density distribution on t^2_{str}. We again use the high-metallicity abundances, and take $\log T_{eff} = 4.85$. We consider several values of n_0 and d_0.

Our results are given in Table 3, where the first and second columns list n_0 and d_0 (in cm), respectively. The third column shows the maximum density occurring in the model. The fourth column gives the value of t^2_{str} for each model. As with our previous density distributions, Table 3 shows the general trend of decreasing t^2_{str} with increasing density. We also note that for a given n_0, models with a larger range in density (i.e., larger n_{max}) have a smaller t^2_{str}. This is because of sphericity effects. The models with larger densities have smaller Strömgren radii, which causes t^2_{str} to decrease through the volume element. This effect essentially negates the greater variation of temperature in these models. The models with $n_0 = 10^6$ do not show this effect since they are plane parallel and thus insensitive to radius.

The results of this section suggest that variable density models will not produce values of t^2_{str} that are significantly larger than those obtained from constant density models, largely because of the strong weighting of t^2_{str} toward high densities. Although this weighting can be removed by choosing a density distribution such as that discussed above, sphericity effects will constrain the magnitude of t^2_{str} obtained. In addition, such a density distribution is somewhat contrived. We thus conclude that although variations in density can produce

TABLE 3

RESULTS OF "CONDENSATION" MODELS

n_0	d_0	n_{max}	t^2_{str}
1.00(2)......	1.00(20)	1.05(2)	3.58(−2)
1.00(2)......	1.00(17)	1.32(5)	7.39(−3)
1.00(3)......	1.00(19)	1.09(3)	1.92(−2)
1.00(3)......	5.00(15)	1.44(6)	4.31(−3)
1.00(4)......	1.00(18)	1.10(4)	6.65(−3)
1.00(4)......	2.00(14)	7.14(6)	6.93(−4)
1.00(5)......	5.00(16)	1.08(5)	3.28(−3)
1.00(5)......	2.00(12)	8.12(7)	6.19(−4)
1.00(6)......	2.00(15)	1.04(6)	5.61(−4)
1.00(6)......	2.00(10)	2.15(8)	1.26(−3)

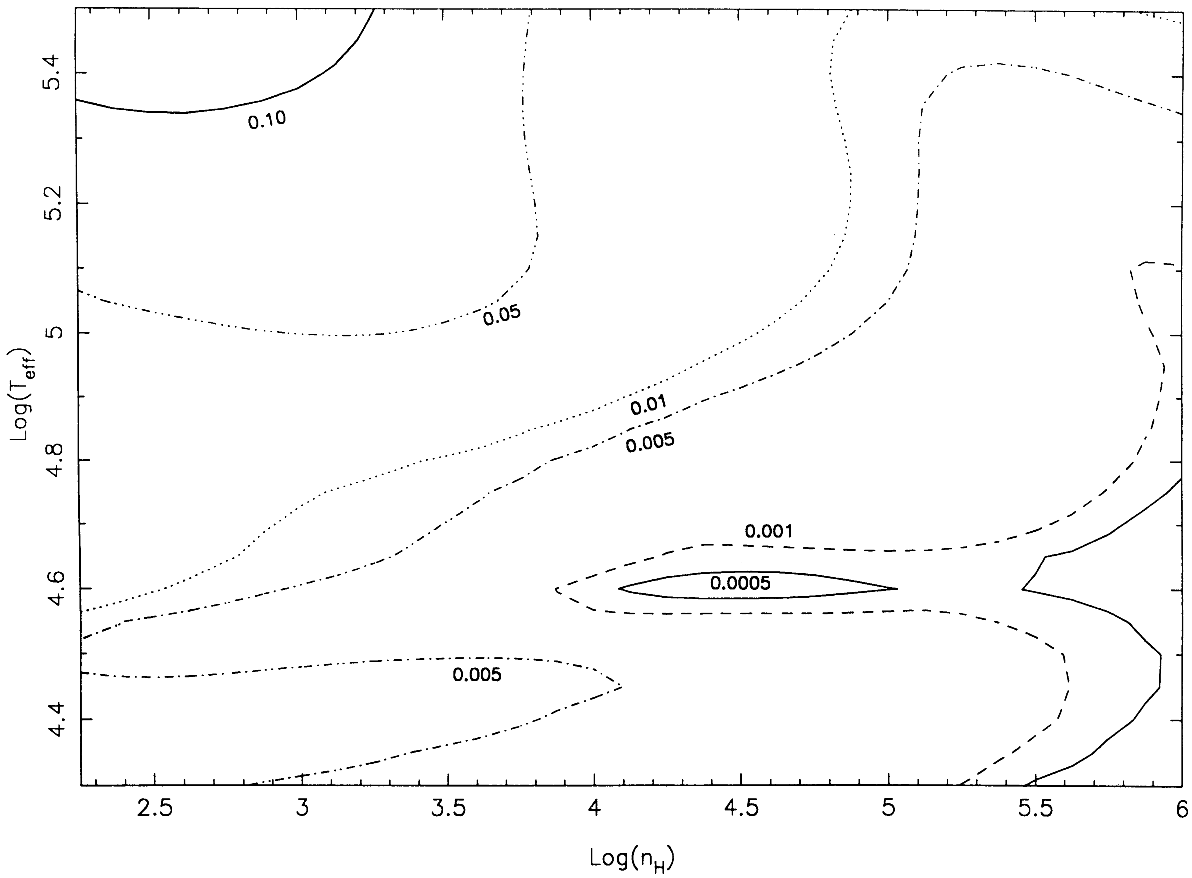

FIG. 8.—Contour plot of t^2_{str} for the high-metallicity grid

variations in temperature, these variations will have little effect on the derived value of t^2_{str}.

4. DISCUSSION

In this section, we discuss the ramifications of our results, and examine the extent to which temperature fluctuations can resolve the abundance discrepancy.

The results of our models demonstrate that t^2 derived from a comparison of [O III] and Balmer temperatures is uncorrelated with t^2 determined directly from the definition. This is due to the fact that the underlying assumption implicit in the derivation of the observed t^2 (i.e., that the radial dependence of temperature is identical in the O^{+2} and H^+ zones) is generally not valid. This assumption can provide a reasonable estimate for nebulae with cooler central stars such as H II regions, but will result in spurious values for objects with hot central stars such as PNs. Even for H II regions, we have shown that slight errors in T(O III) and T(Bal) can result in significant errors in t^2, so that the derived value will be subject to considerable uncertainty.

This situation is unfortunate, as it implies that there is no sure way to determine t^2 observationally from nebular spectra when the O^{++} and H^+ zones do not coincide. In addition to the T(O III)–T(Bal) approach, two other methods have been used to derive t^2 observationally. We briefly discuss these methods and their associated problems below.

The first method compares T(O III) with a radio temperature determined from the ratio of a bound-bound H radio line with the radio continuum (see Rubin 1969 and Torres-Peimbert et al. 1980 for applications of this method). It is clear that this method requires the exact same assumption as the T(O III)–T(Bal) approach, and thus has the identical problems with validity. Moreover, the need to connect radio and optical data will result in additional observational uncertainty.

One way to avoid the problems inherent in both the T(O III)–T(Bal) and T(O III)–T(Radio) methods is to use two different temperature indicators from one ion. This technique was utilized by Dinerstein et al. (1985), who used the temperature based on [O III] $\lambda5007/\lambda4363$, as well as the temperature based on [O III] 5007/52 μm. While this approach does away with the assumption necessary in the other two methods, it does have some problems of its own. Observationally, there are two concerns: (1) The need to compare optical and infrared (IR) lines requires an accurate knowledge of the amount and form of the reddening in the object; and (2) It is essential to use identical apertures for the IR and optical spectra, in order to ensure that the same total flux is received. Theoretically, this method is hampered by the low critical density of the [O III] 52 μm line ($\sim 3.8 \times 10^3$). Therefore, although this method should produce accurate results for low-density nebulae, provided great care is taken in the observations, it is essentially useless for higher density objects.

Perhaps the best way to determine t^2 observationally would be to use a high-resolution imaging device such as a Fabry-Perot. The technique would consist of mapping temperature-sensitive line ratios across the face of the nebula (see, e.g., Lame & Pogge 1994). Unfortunately, this method would only be

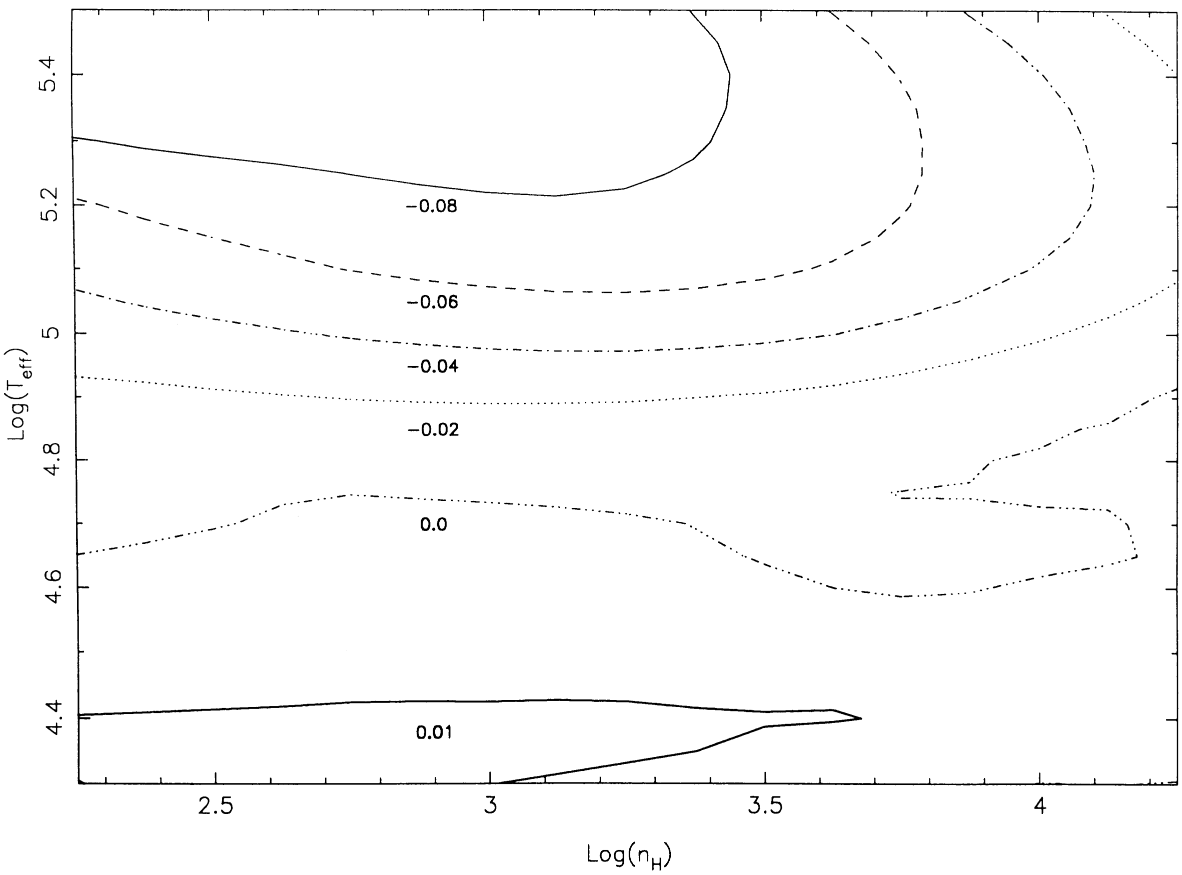

FIG. 9.—Contour plot of the difference $t^2_{obs} - t^2_{str}$ for the high-metallicity grid

useful for relatively nearby objects which could afford high spatial resolution.

We now return to the main purpose of this investigation, that is, to determine whether temperature fluctuations can resolve the discrepancy between recombination-line abundances and forbidden-line abundances. We have seen in § 3 that relatively large values of $t^2(H^+)$ can occur for nebulae with low density, hot central stars, and high metallicity. However, if we are interested in determining the abundance of an element A in the ith stage of ionization, what we really need to examine is not $t^2(H^+)$, but $t^2(A_i)$. For example, in NGC 7009, the bulk of O is in the form O^{+2}, so in order to resolve the discrepancy between the O^{+2} abundance measured from O III forbidden lines and O II recombination lines, we require a large value of $t^2(O^{+2})$. The models of Harrington et al. (1982) show that $t^2(A_i) < t^2(H^+)$, since A_i occupies a smaller volume than H^+. Tests with our grids verify that in general $t^2(O^{+2}) < t^2(H^+)$, but in a few cases we can have $t^2(O^{+2}) > t^2(H^+)$. These cases occur for objects with log $T_{eff} \sim 4.6$, typical of high-excitation H II regions. These nebulae have O primarily in the form O^{+2}, giving way to O^+ in the outer regions. The temperature decreases with radius in the O^{+2} zone, but rises slightly in the O^+ zone because of the absence of strong coolants. This rise decreases the temperature gradient over the whole H^+ zone compared with the O^{+2} zone, causing $t^2(O^{+2}) > t^2(H^+)$. However, in these cases, $t^2(O^{+2})$ is generally less than a factor of ~ 2 greater than $t^2(H^+)$, and as Figures 2 and 8 show, the value of $t^2(H^+)$ for log $T_{eff} \sim 4.6$ is relatively small. In general, we find that $t^2(O^{+2})$ will have a maximum value on the order of 10^{-2} over the range of densities and stellar temperatures considered. These values are insufficient to resolve the abundance discrepancies.

In order to quantify these expectations, we use the constant density PN grid from § 3 to calculate the relative abundance of O^{+2}. We derive abundances from the expression

$$\frac{O^{+2}}{H^+} = \frac{5007}{4861} \frac{\alpha^{eff}_{H\beta}(T)}{q_{^3P,^1D} B[1 + (n_e q_{^1D,^3P}/A_{^1D,^3P})]^{-1}} \frac{I(5007)}{I(H\beta)} , \tag{12}$$

where $\alpha^{eff}_{H\beta}(T)$ is the effective recombination coefficient for Hβ, the q's are collisional rate coefficients, and B is the branching ratio, i.e., the fraction of radiative decays from ^1D that produce λ5007. The factor in brackets is a correction for collisional de-excitation.

For $\alpha^{eff}_{H\beta}(T)$, we have determined a power-law fit in temperature from the results of Hummer & Storey (1987) at a density of 10^4 cm^{-3}. Because of the weak density dependence of $\alpha^{eff}_{H\beta}(T)$, this choice of density will not affect our results. Similarly, we have made a power-law fit in temperature to the collision strength $\Omega_{^3P,^1D}$ from the data of Aggarwal (1993). The A- and B-values were obtained from Osterbrock (1989). Substituting in these values yields

$$\frac{O^{+2}}{H^+} = 1.8 \times 10^{-4} T_{H\beta}^{-0.864} T_{5007}^{0.373} \exp\left(\frac{2.888 \times 10^4}{T_{5007}}\right) \times [1 + 1.4 \times 10^{-4} n_e(O^{+2}) T_{5007}^{-0.5}] \frac{I(5007)}{I(H\beta)} , \tag{13}$$

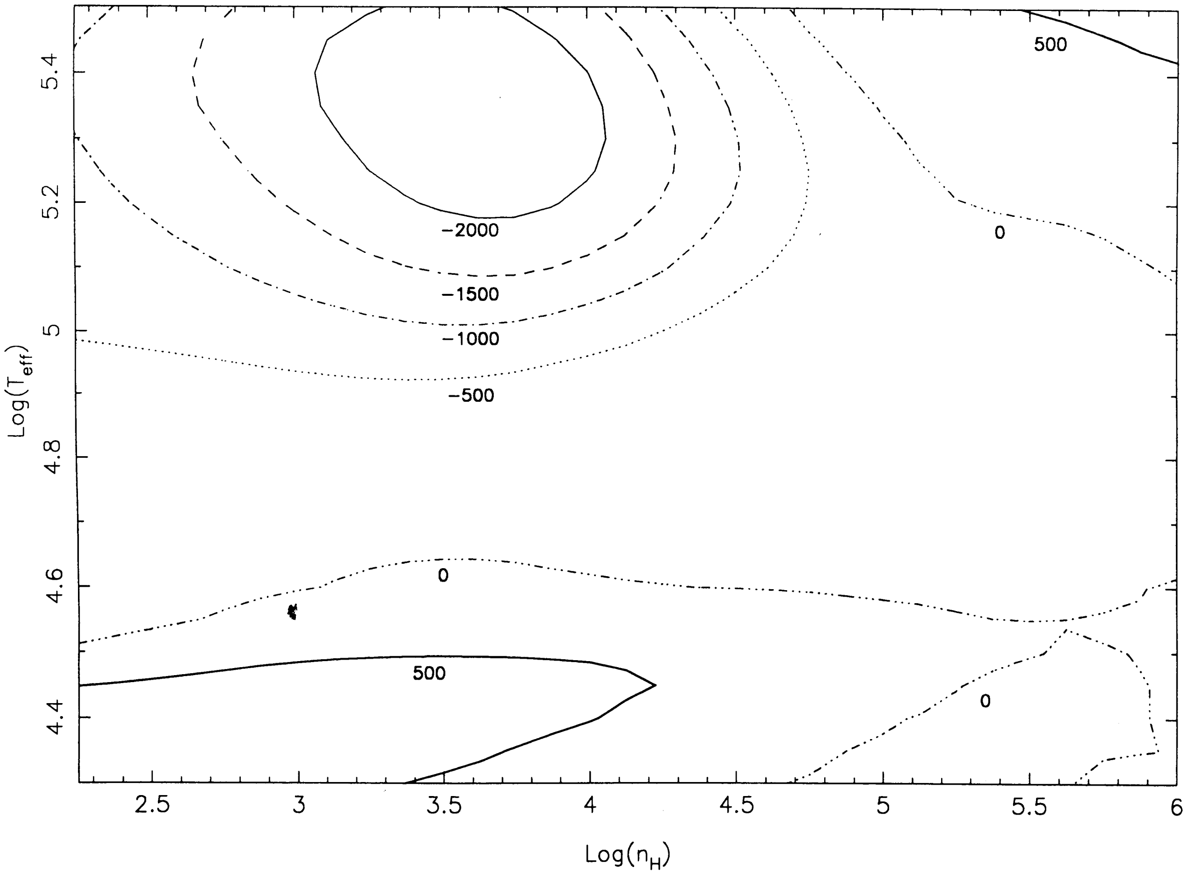

FIG. 10.—Contour plot of the difference $T_0(O^{+2}) - T_0(H^+)$ for the high-metallicity grid

where $T_{H\beta}$ and T_{5007} are the temperatures in Hβ and [O III] λ5007, respectively.

We then calculate (O^{+2}/H^+) in two ways. First, we use the standard method of simply substituting T(O III) for both T_{5007} and $T_{H\beta}$ in equation (13). This approach assumes that $t^2 = 0$. Second, we explicitly take account of temperature fluctuations by using the appropriate values of T_{5007} and $T_{H\beta}$. Peimbert (1967) has shown that in the presence of temperature fluctuations, T_{5007} is related to $T_0(O^{+2})$ and $t^2(O^{+2})$ through the equation

$$T_{5007}^{-0.5} \exp\left(\frac{2.888 \times 10^4}{T_{5007}}\right) = T_0^{-0.5}(O^{+2}) \exp\left[\frac{2.888 \times 10^4}{T_0(O^{+2})}\right] \times \left[1 + \left\{\left[\frac{2.888 \times 10^4}{T_0(O^{+2})}\right]^2 - \frac{8.664 \times 10^4}{T_0(O^{+2})} + \frac{3}{4}\right\} \frac{t^2(O^{+2})}{2}\right] . \quad (14)$$

Similarly, using our power-law equation for $\alpha_{H\beta}^{\rm eff}(T)$ yields

$$T_{H\beta} = T_0(H^+)[1 - 0.932t^2(H^+)] . \quad (15)$$

Our results for each model are shown in Table 4, where the first and second columns give log n_H and log $T_{\rm eff}$, respectively. The third column shows T(O III), corrected for collisonal de-excitation and noncollisional effects in [O III] λ4363. Both of these effects are small for the models considered here. The fourth and fifth columns give the model-predicted values of $T_0(O^{+2})$ and $t^2(O^{+2})$, respectively, and the sixth column gives the value of T_{5007} derived from equation (14). Similarly, the seventh and eighth columns show $T_0(H^+)$ and $t^2(H^+)$, respectively, with the ninth column giving the value of $T_{H\beta}$ from equation (15). The (O^{+2}/H^+) abundance ignoring temperature fluctuations [i.e., using only T(O III)] is shown in the tenth column, and the (O^{+2}/H^+) abundance taking temperature fluctuations into account (i.e., using T_{5007} and $T_{H\beta}$) is shown in the eleventh column. Finally, the ratio of the eleventh column to the tenth column is given in the last column. This is essentially the abundance correction factor.

We note two points of interest from our results. First, for the models considered in Table 4, the correction for temperature fluctuations is quite small, with a maximum value $\sim$3%. Second, for several models, the ratio R in the last column is less than 1. For these cases, ignoring the effects of temperature fluctuations actually results in an *overestimate* of the O^{+2} abundance. These models all have $t^2(H^+) \gg t^2(O^{+2})$, and $T_{H\beta} >$ T(O III). This causes the $T_{H\beta}$ term in equation (13) to outweigh the exponential.

Table 4 clearly shows that while the values in the last column can be non-negligible corrections for some purposes, they are far insufficient to explain the factor of 2 for several objects, or the factor of 5 in NGC 7009 necessary to reconcile recombination-line and forbidden-line abundances. Somewhat larger values can be obtained from high-metallicity objects, but these are also far short of the needed factors.

It is difficult to imagine how to significantly increase t^2. Physically, the problem results from the strong increase in the cooling curve with temperature over the temperature range applicable to gaseous nebulae. In order to produce a given change ΔT in the temperature, it is necessary to have a signifi-

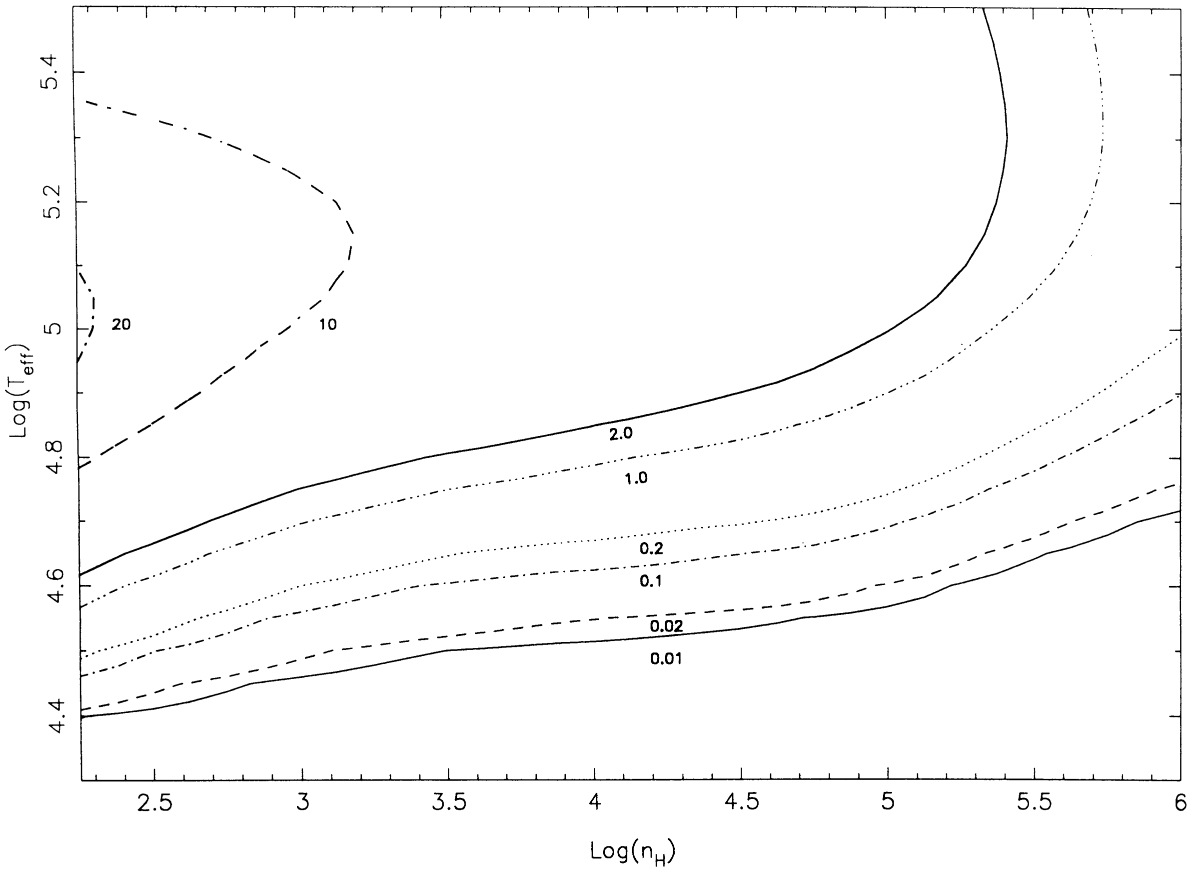

FIG. 11.—Percentage of the [O III] $\lambda4363$ intensity due to noncollisional processes for the high-metallicity grid

cantly larger change ΔH in the nebular heating. As a concrete example, consider a nebula with $T_0 = 10^4$ K and $t^2 = 0.04$, corresponding to a 20% variation in the temperature. For simplicity, let us assume that the cooling is entirely due to [O III] $\lambda5007$. Then the resulting percentage variation in the total cooling, $\Delta C/C$, is roughly 50%. In thermal equilibrium, this is equivalent to the percentage variation in nebular heating, $\Delta H/H$. A situation where the heating can vary by this large an amount is difficult to produce physically.

While several other ideas such as high-density condensations (see Viegas & Clegg 1994) have been proposed to explain the abundance discrepancy, the issue remains unresolved. Since the discrepancy amounts to less than a factor of 2 for most objects, it may be that NGC 7009 is peculiar in some way. As mentioned in § 1, the CNO recombination-line abundances for this object are strongly enhanced relative to solar. Further study of this object would be useful toward resolving this discrepancy.

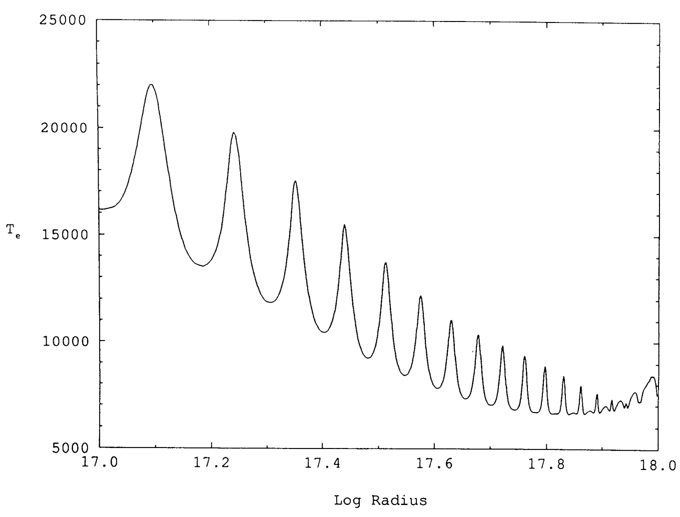

FIG. 12.—Variation of temperature with radius for a sinusoidally varying density.

5. SUMMARY

We summarize the main findings of this study below.

1. The commonly used value of t^2 derived from a comparison of T(O III) and T(Bal) is uncorrelated with the t^2 determined from theory, and should not in general be used. It can provide a reasonable estimate for objects with low stellar temperatures, but is subject to large uncertainties. The T(O III)–T(Radio) method is equally poor. Given precise observational data, the method of Dinerstein et al. (1985) should provide accurate results, but is only useful for low-density objects.

2. In general, for any ion A_i, $t^2(A_i)$ increases with increasing metallicity.

3. While density fluctuations can create fluctuations in temperature, these will not significantly affect t^2 because of the strong weighting toward higher densities.

4. Although temperature fluctuations can produce non-negligible abundance corrections for some objects, they are

TABLE 4

ABUNDANCES FROM DIFFERENT TEMPERATURES

log n_H	log $T_{\rm eff}$	T(O III)	$T_0(O^{+2})$	$t^2(O^{+2})$	T_{5007}	$T_0(H^+)$	$t^2(H^+)$	$T_{H\beta}$	O^{+2}/H^{+a}	O^{+2}/H^{+b}	R
2.5......	4.6	7.335(3)	7.273(3)	1.554(−3)	7.280(3)	7.458(3)	2.292(−3)	7.442(3)	1.68(−4)	1.70(−4)	1.01
2.5......	4.9	9.663(3)	9.522(3)	4.336(−3)	9.529(3)	9.776(3)	9.336(−3)	9.691(3)	3.30(−4)	3.41(−4)	1.03
2.5......	5.2	1.225(4)	1.213(4)	3.161(−3)	1.212(4)	1.279(4)	2.662(−2)	1.247(4)	2.40(−4)	2.42(−4)	1.01
3.0......	4.6	7.820(3)	7.760(3)	1.258(−3)	7.765(3)	7.856(3)	1.359(−3)	7.846(3)	2.03(−4)	2.07(−4)	1.02
3.0......	4.9	1.014(4)	1.003(4)	3.658(−3)	1.003(4)	1.026(4)	9.105(−3)	1.017(4)	3.49(−4)	3.58(−4)	1.02
3.0......	5.2	1.262(4)	1.249(4)	3.689(−3)	1.248(4)	1.349(4)	3.205(−2)	1.309(4)	2.36(−4)	2.34(−4)	0.99
3.5......	4.6	8.198(3)	8.158(3)	8.018(−4)	8.161(3)	8.227(3)	9.237(−4)	8.220(3)	2.41(−4)	2.44(−4)	1.01
3.5......	4.9	1.056(4)	1.046(4)	3.478(−3)	1.046(4)	1.068(4)	8.170(−3)	1.060(4)	3.65(−4)	3.72(−4)	1.02
3.5......	5.2	1.295(4)	1.281(4)	4.618(−3)	1.280(4)	1.419(4)	3.365(−2)	1.374(4)	2.30(−4)	2.24(−4)	0.97
4.0......	4.6	8.402(3)	8.364(3)	3.296(−4)	8.365(3)	8.459(3)	7.999(−4)	8.453(3)	2.58(−4)	2.61(−4)	1.01
4.0......	4.9	1.078(4)	1.068(4)	3.325(−3)	1.068(4)	1.084(4)	5.496(−3)	1.078(4)	3.84(−4)	3.93(−4)	1.02
4.0......	5.2	1.312(4)	1.296(4)	5.726(−3)	1.294(4)	1.445(4)	2.640(−2)	1.409(4)	2.33(−4)	2.25(−4)	0.96

[a] Derived from T(O III).
[b] Derived from T_{5007} and $T_{H\beta}$.

insufficient to resolve the discrepancy between recombination-line and forbidden-line abundances.

5. Noncollisional effects in [O III] λ4363 can have important effects on the derived [O III] temperature. This is especially true for high-metallicity objects.

We are indebted to X.-W. Liu for a discussion on the determination of abundances in the presence of temperature fluctuations. We also thank the referee for pointing out an earlier error in one of the equations. This research was supported by NSF 93-19034 and NASA NAGW-3315.

REFERENCES

Aggarwal, K. M. 1993, ApJS, 85, 197
Aller, L. H. 1990, PASP, 102, 1097
Aller, L. H., & Czyzak, S. J. 1983, ApJS, 51, 211
Baldwin, J. A., Ferland, G. J., Martin, P. G., Corbin, M. R., Cota, S. A., Peterson, B. M., & Slettebak, A. 1991, ApJ, 374, 580
Barlow, M. J., Clegg, R. E. S., Liu, X.-W., & Storey, P. J. 1995, MNRAS, in press
Barker, T. 1979, ApJ, 227, 863
Borkowski, K. J., & Harrington. J. P. 1991, ApJ, 379, 168
Dinerstein, H. L., Lester, D. F., & Werner, M. W. 1985, ApJ, 291, 561
Dalgarno, A., & Sternberg, A. 1982, ApJ, 257, L87
Ferland, G. J. 1980, PASP, 92, 596
Ferland, G. J. 1994, Hazy, University of Kentucky Department of Physics and Astronomy Internal Report
Harrington, J. P., Lutz, J. H., Seaton, M. J., & Stickland, D. J. 1980, MNRAS, 191, 13
Harrington, J. P., Seaton, M. J., Adams, S., & Lutz, J. H. 1982, MNRAS, 199, 517
Harrington, J. P., Monk, D. J., & Clegg, R. E. S. 1988, MNRAS, 231, 577
Hummer, D. G., & Storey, P. J. 1987, MNRAS, 224, 801
Lame, N. J., & Pogge, R. W. 1994, AJ, 108, 1860
Liu, X.-W., & Danziger, J. 1993, MNRAS, 263, 256
Liu, X.-W., Storey, P. J., Barlow, M. J., & Clegg, R. E. S. 1995, MNRAS, 272, 369
Kingdon, J., & Ferland, G. J. 1993, ApJ, 403, 211
Mallik, D. C. V., & Peimbert, M. 1988, Rev. Mexicana Astron. Af., 16, 111
Middlemass, D., Clegg, R. E. S., Walsh, J. R., & Harrington, J. P. 1991, MNRAS, 251, 284
Mihalszki, J. S., & Ferland, G. J. 1983, PASP, 95, 284
Osterbrock, D. E. 1989, Astrophysics of Gaseous Nebulae and Active Galactic Nuclei (Mill Valley, CA, University Science Books)
Peimbert, M. 1967, ApJ, 150, 825
Rubin, R. H. 1969, ApJ, 155, 841
———. 1986, ApJ, 309, 334
———. 1989, ApJS, 69, 897
Shaver, P. A., McGee, R. X., Newton, L. M., Danks, A. C., & Pottasch, S. R. 1983, MNRAS, 204, 53
Shields, G. A. 1990, ARA&A, 28, 525
Stasińska, G. 1980, A&A, 85, 359
Torres-Peimbert, S., Peimbert, M., & Daltabuit, E. 1980, ApJ, 238, 133
Torres-Peimbert, S., Peimbert, M., & Peña, M. 1990, A&A, 233, 540
Viegas, S. M., & Clegg, R. E. S. 1994, MNRAS, 271, 993
Williams, R. E. 1992, ApJ, 392, 99